Exoplanetary Candidates Around HD100546 in Archival ACS Data

Elisabeth Frischknecht

A senior thesis submitted to the faculty of
Brigham Young University
in partial fulfillment of the requirements for the degree of

Bachelor of Science

Denise Stephens, Advisor

Department of Physics and Astronomy

Brigham Young University

ABSTRACT

Exoplanetary Candidates Around HD100546 in Archival ACS Data

Elisabeth Frischknecht
Department of Physics and Astronomy, BYU
Bachelor of Science

Herbig Ae/Be (HAeBe) stars are classified as 2-10 solar mass pre-main sequence stars with protoplanetary disks. As a result, they are excellent candidates for observing exoplanets in the formative stages of their evolution. By constructing and then subtracting a model Point Spread Function from object frames, an image of the protoplanetary disk and any planets located within it is obtained. This technique was used to analyze archival Hubble Space Telescope images of HAeBe object HD100546, which is known to host at least one planet (HD100546b) that has been detected at near-infrared wavelengths by other telescopes. The supposed detection of HD100546b is likely a false positive, but it is possible that the planet is still located within the data and may be detectable upon further research.

Keywords: Protoplanetary Disks, PSF Subtraction, HD100546, Exoplanets, PynPoint, Principle Component Analysis

ACKNOWLEDGMENTS

First, I would like to thank Dr. Denise Stephens for her mentorship on this project. Her guidance was invaluable, and she is a role model in every sense. Second, I'd like to thank my family for the love and support throughout the years. I'd also like to acknowledge the College of Physical and Mathematical Sciences for their funding of this project, and the Office of Research and Creative Activities (ORCA) for their additional support. This work would not have been possible without each of you.

Contents

Table of Contents **iv**

1 Introduction **1**
1.1 Solar System Formation and Protoplanetary Disks 1
1.2 Point Spread Functions and Coronagraphic Images 4
1.3 Previous Work 6
1.4 Overview 8

2 Methods **10**
2.1 Archival Data 10
2.2 PSF Subtraction 13
2.3 PynPoint 14

3 Results **18**
3.1 Analysis and Conclusions 18
3.2 Directions for Further Work 20

Appendix A Basis Images **23**

Bibliography **32**

Index **33**

Chapter 1

Introduction

1.1 Solar System Formation and Protoplanetary Disks

Planet formation around massive stars is not well understood, so we are probing early stages of planet and star formation to better understand planet formation timescales around these objects.

The prevailing theory of solar system formation begins with a large cloud comprised of hydrogen, helium, and some heavier metals. These clouds are stable with the inward force of gravity being balanced by outward gas pressure. However, if a shock wave disturbs the stability of the cloud it will freely collapse under the force of gravity. Even the smallest amount of angular momentum present before the collapse will cause the entire cloud to rotate and eventually flatten into a disk. Conservation of energy converts the gravitational potential energy into the kinetic energy of the particles, causing them to heat up as they fall toward the center of the collapse. At the center of the disk, material will begin to condense into a star while the outer regions will become what is called a protoplanetary disk.

The protoplanetary disk is the home of planet formation. In the early stages of solar system formation, individual particles will combine to make larger dust grains. These dust grains will

continue to collide and coalesce until they become large enough to be called planetesimals. As the planetesimals accrete material, they leave empty trails in the protoplanetary disk, known as formation tracks. The dark ring-like structures seen in Fig.1.1 show the presence of several formation tracks within the protoplanetary disk of a single star. The presence of each track is thought to indicate a future planet that will reside within the exoplanetary system. For the region of the protoplanetary disk that lies close to the star, the force of gravity must compete with the solar wind, a continuous flow of particles emanating from the sun. This radially propagating force pushes lighter elements away, so that the planets will be comprised primarily of heavier elements. These objects will become terrestrial planets, like the earth. Farther away from the star, the solar wind has a lesser effect so the lighter elements, such as gasses, will accrete onto the rocky planetesimal bodies. This results in large gas giants, called Jovian planets, such as Jupiter.

In our solar system, the progression of terrestrial to Jovian planets follows a simple trend, with rockier planets residing close to the host star and Jovian planets being further away. This holds with the current theories on solar system formation. However, the Kepler[1] mission revealed that this trend isn't necessarily true for extrasolar systems. Many systems have been discovered that contain what are called "Hot Jupiters". These planets are gas giants on the same size scale as Jupiter but which orbit incredibly close to the host star. It is unlikely that the Hot Jupiters formed in these tight orbits, so we are left to wonder at how they arrived in their current positions. The prevailing theory is that a third body, most likely a planet, causes a gravitational interaction forcing the Hot Jupiter to migrate inward. Barring the presence of another planet, the protoplanetary disk could potentially act as the third body providing the interaction. Observing planets, particularly gas giants, in their formation period would provide invaluable constraints on the details of this process.

The search for exoplanets has historically been constrained to solar-type stars, but Herbig Ae/Be (HAe/Be) stars offer promising results. HAe/Be stars are classified as 2-10 solar mass ($M_{\odot}$)

[1] https://www.nasa.gov/mission_pages/kepler/overview/index.html

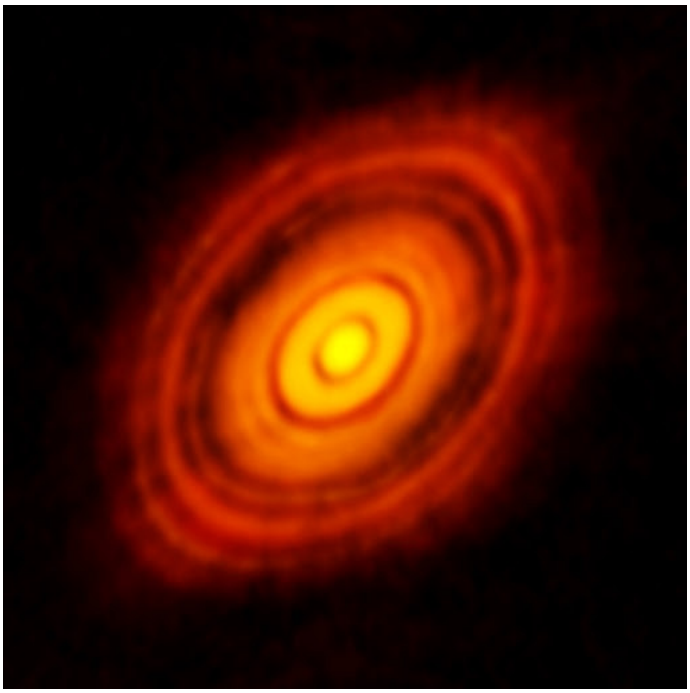

Figure 1.1 The image of a protoplanetary disk from the Atacama Large Millimeter Array (ALMA). The formation tracks of planets can be clearly seen within the image. Image Credit: ALMA (ESO/NAOJ/NRAO) - http://www.eso.org/public/images/eso1436a/

pre-main sequence stars with protoplanetary disks. The disks of HAe/Be stars are much brighter and larger than those found around solar-type stars. Additionally, they are easier to observe over a wide range of wavelengths (Quanz 2015), which makes it possible to detect more disk features. These properties make HAe/Be stars excellent candidates for observing forming planets. However, the disks of HAe/Be have been studied relatively little compared to other star types with planetary disks, such as T-Tauri stars. For these reasons, we decided to investigate the disks of HAe/Be stars and search for any planets that may be located within them.

1.2 Point Spread Functions and Coronagraphic Images

The direct imaging of planets within protoplanetary disks is easier said than done. After the planets and the host star are essentially formed, the protoplanetary disk enters the debris disk phase. The debris disk contains a lot of extraneous dust, gas, and debris that will one day become asteroids or similar objects. Although there is still a lot of material contained within the protoplanetary disk, the planets that have formed are now theoretically detectable within the formation tracks. However, compared to the luminosity of the star, planets are very dim. At visible wavelengths a star can be a billion times brighter than the planet around the star, and a million times brighter in the near-infrared. Additionally, the dust grains within the disk glow brightly in similar wavelengths to the planets, so it can be difficult to detect the planets amidst the noise of the disk. Only cameras with high resolution power are capable of detecting these objects due to the small size of the planets. As a result, only a handful of attempts to directly image exoplanets in protoplanetary disks have been successful (Espaillat 2019).

Coronagraphs are a special telescope attachment that aide in the imaging of protoplanetary disks. As starlight enters the telescope during an observation, the natural spreading of starlight as it passes through the optics washes out any faint emission being given off by the disk around the star or any

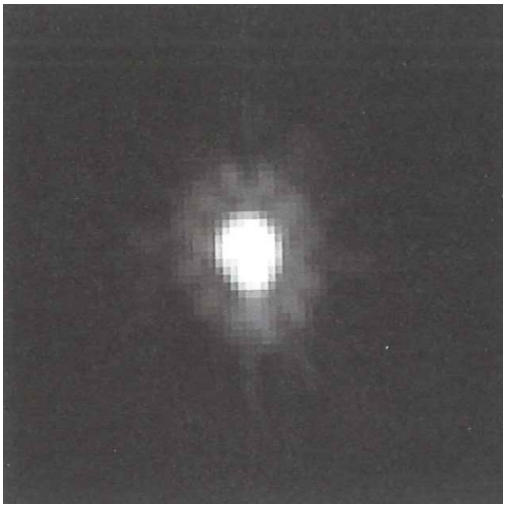

(a) PSF without coronagraphic mask.

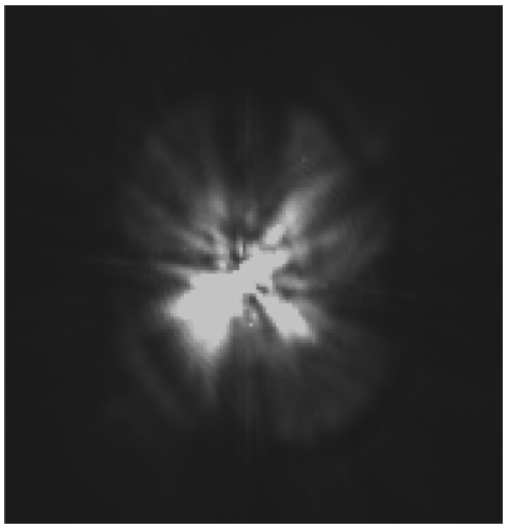

(b) PSF with coronagraphic mask.

Figure 1.2 Two images of the same object with and without the coronagraphic mask

light emitted by a forming planet in the disk . This spread of light is called a Point Spread Function, or PSF. To see planets and disks around the star, we place a coronagraph in front of the star to block its light. While the coronagraph blocks a large fraction of the host star's light, it introduces an irregular diffraction pattern that contributes to the PSF of the image. Fig 1.2a (Safsten Brigham Young University, Provo, U.T., 2017) shows the PSF of a star observed without a coronagraphic mask, while Fig 1.2b shows a PSF of a star with the coronagraph in place. The PSF in Fig 1.2b is clearly much noisier due to the diffraction of the light.

Coronagraphic PSFs are predictable and can be modeled using various techniques. Typically, observations taken of standard stars can be used to generate the model PSF. Stars of similar type and class will generate light in similar ways. If enough images are used, they will form a basis set that can be stacked and averaged to create a model PSF. This model PSF can then be compared to the object's PSF to remove the effects of the complex PSF from the residual images. Speckle patterns and noise will still remain that may hide the presence of a planet or create a false positive

identification. PSF subtraction will be further discussed in section 2.2.

1.3 Previous Work

The first, and only, confirmation of a planet in the disk of a HAe/Be star was found around HD100546. Fig 1.4 shows an image of the protoplanetary disk and highlights the location of the planet. HD100546 is a relatively young $2.4M_{\odot}$ star (van den Ancker et al. 1997) with a predicted age range of ~5-10 Myr (Guimarães et al. 2006) and $\geq$ 10 Myr by van den Ancker et al. (1997). The disk of HD100546 is quite large, with a radius of over 300 Astronomical Units (AU), where an AU is the average distance between the earth and the sun. There are two prominent gaps, one located at ~14AU (Currie et al. 2014) and another at ~50AU (Quanz 2015). Quanz et al. (2015) was able to recover a planet (HD100546b) within the gap at 50AU. The original discovery paper of HD100546b (Quanz et al. 2013) was unable to confirm the planet because the data was based upon single-wavelength observations. A confirmation paper (Quanz et al. 2015) was later released with data taken in multiple filters. HD100546b is calculated to be ~5-10 $M_{Jupiter}$ and around 1Myr old (Quanz et al. 2015). The residual images of the disk can be seen in Fig. 1.3, where the planet can be clearly seen as the dark red spot in the upper portion of the disk. The second red feature on the left of the $M^{'}$ band is likely a spiral arm feature of the disk and is not a planet.

The HD100546 system is of particular interest to us because there may potentially be a undiscovered planet located within the protoplanetary disk (HD100546c). Currie et al. (2014) detected a gap in the disk around HD100546 at 14AU that may indicate the presence of a second planet in the system. However, Currie et al. (2014) were unable to detect a planet within the gap at 14AU, though they were also able to recover HD100546b as well as the disk feature seen in Fig 1.3. If HD100546c (which is projected to be a large Jovian planet) is detected, it would allow us to observe the formation of multiple Jovian planets at both near and far separations from the host star. In

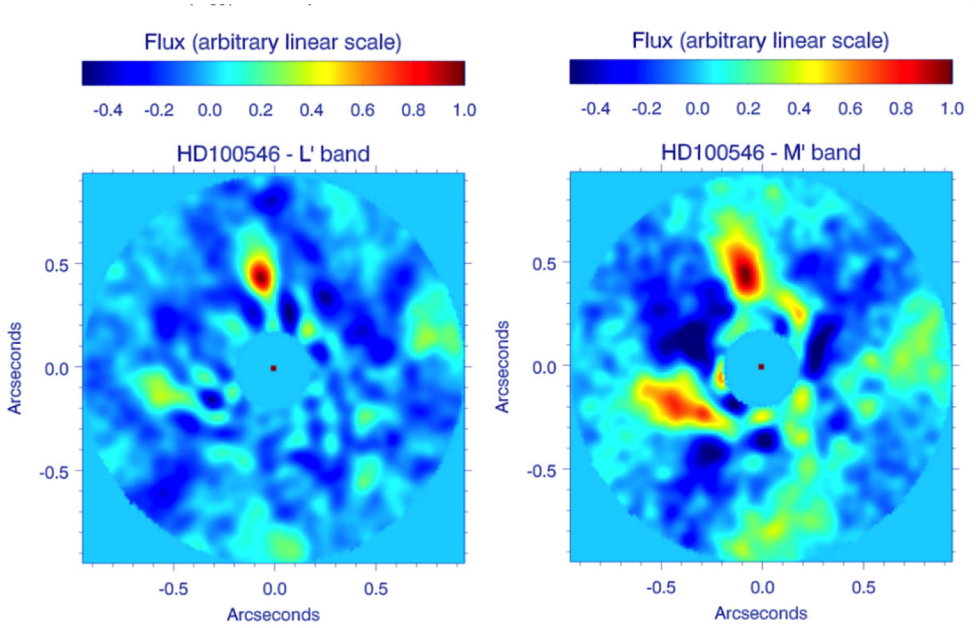

Figure 1.3 Taken from Quanz et al., 2014. This image shows the confirmed planet HD100546b in two filters. These are residual images of the disk that are produced using PSF subtraction methods.

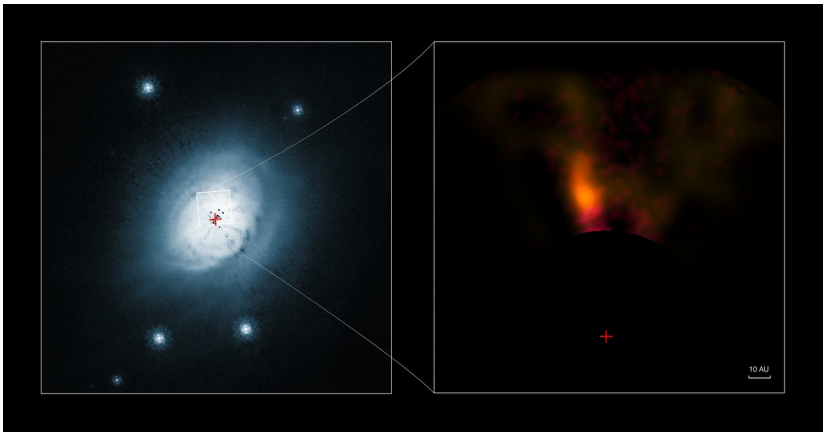

Figure 1.4 Image of the disk of HD100546, with the enlarged portion showing the proposed planet (citation).

the field of astronomy, this is as close to a perfect laboratory experiment as can be achieved. The HD100546 system could be invaluable to our understanding of planet formation.

A previous master's student at BYU, Emily Safsten, analyzed the archival data of many HAe/Be

stars using PSF subtraction. Her work focused on using archival data as a screening tool to find objects that warrant taking a second look. However, in her analysis of HD100546 Emily may have detected the presence of HD100546c (Safsten Brigham Young University, Provo, U.T., 2017). The PSF subtraction residual images are seen in Fig 1.5. HD100546b can be seen as a small dark red dot in the top of Fig 1.5a, while the proposed HD100546c can be seen in the left of Fig 1.5b. The difference between these two images comes from the orientation angle of the telescope, which may allow us to probe different layers of the protoplanetary disk. However, there are many reasons to doubt this detection. First, these images were taken in optical wavelengths of light while planets are typically easiest to find in the infrared. Second, the data seen in the residual images is very noisy (particularly when compared to the residuals in Fig 1.3) and it is difficult to say if the "detection" is really noise in the disk. Third, the algorithm used to perform the PSF subtraction is highly aggressive and could easily have generated a false positive within the residual images. Fourth, the angular resolution of the coronagraph must be taken into consideration as HD100546c is located fairly close to the host star. Although we are skeptical of this detection, the discovery of HD100546c would provide us with much needed information on the formation of solar systems. Consequentially, much of the research we have conducted has been an effort to confirm these results.

1.4 Overview

Chapter 2 of this thesis will cover the methods used to confirm the detection of HD100546c, including the nature of archival data, PSF subtraction and Principle Component Analysis, the software PynPoint, and the steps taken to analyze the data itself. Chapter 3 covers the results and conclusions of the methods section, as well as providing suggestions for future work in this field.

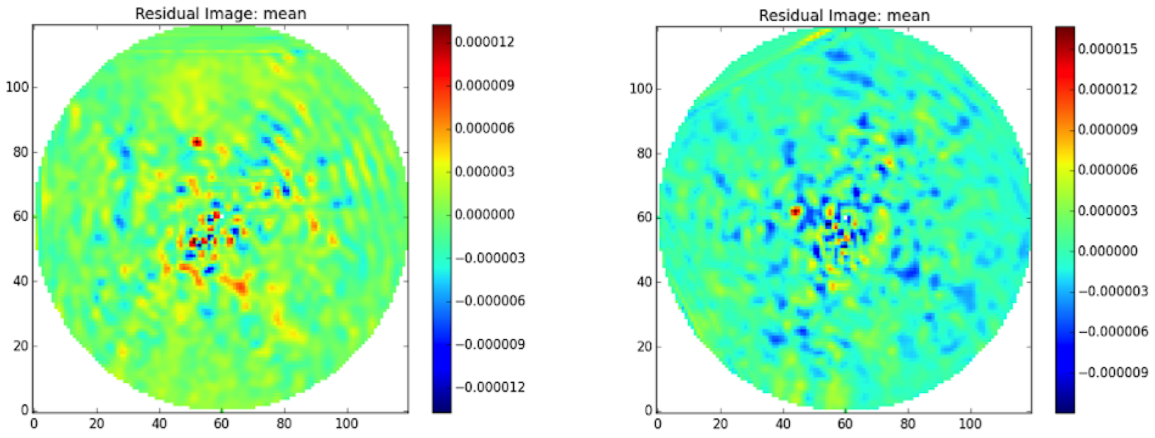

(a) The confirmed planet, HD100546b **(b)** The candidate planet, HD100546c

Figure 1.5 Residual images taken from the thesis of Emily Safsten. These images show what is believed to be the confirmed planet HD100546b and the proposed planet HD100546c.

Chapter 2

Methods

2.1 Archival Data

The study of protoplanetary disks is not a recently developed field; many coronagraphic observations of young stars with disks already exist. Much of this data is held in archives that are available for public use. During the time that these observations were taken, the focus of the research was on studying and categorizing the features of the protoplanetary disks and not on detecting exoplanets. As a result, much of the archival data is not optimized for the analyses that we are conducting. Nevertheless, these data still serve a purpose in our research.

One of the major problems associated with directly imaging exoplanets is choosing objects to observe. Simply pointing a telescope at a random object hoping to detect a planet is highly inefficient and costly. Archival data can be used to mitigate this problem by serving as a screening tool for flagging objects that warrant closer investigation and follow up observations.

Advanced signal processing techniques now make it possible to go back through archival disk images and look for planets. In the time since the original observations were taken, image processing techniques have advanced significantly. These advances allow for more accurate modeling of the

Point Spread Function (PSF) and subtraction techniques that may now reveal more detail than before. This information may include the existence of any planets that are located within the protoplanetary disk. The possibility of a new detection is one motivation for taking another look at the coronagraphic images currently being stored in archives. Hubble Space Telescope (HST) data are available to the public, easy to access, and useful to analyze for this project. HST data also work easily with the program we use to perform PSF subtraction, called PynPoint, and have not been used in this type of analysis before. For these reasons, archival data is used to begin our search for planets.

HST observed several stars with protoplanetary disks using the Advanced Camera for Surveys (ACS). It was in this set of data that Safsten (2017) screened for any possible planetary detections. During this screening, HAe/Be star HD100546 stood out with a possible detection of not one, but two exoplanets. With the previous confirmation of one exoplanet in the system (Quanz et al. 2015) and a theorized secondary planet (Currie et al. 2014), this detection called for a deeper investigation.

Observations for HD100546 were taken over ten years ago in two separate proposals, which compose the science, or object, frames of our data set. The first, HST Proposal 9295, took observations of a number of objects with protoplanetary disks, including HD100546. A total of 14 images were taken of HD100546, with eight images using the HRC-CORON1.8 aperture. This aperture is the coronagraphic attachment, so these images will be the focus of this analysis. The specifications of the observations can be seen in Table 2.1, including the date of observation, the exposure time, apertures, and filters used for each image. The subtraction shown in Section 2.2 focused on the the F606W;CLEAR2S filter set. We combined the data from HST proposal 9295 with the data from HST proposal 9987 because they were taken close together in time. Because the centering of ACS drifts over time, images from observations taken close together can be more easily aligned and produce a better PSF subtraction.

ACS data is reduced before being added to the archive, so there is no need to obtain bias frames

(zeroes, darks, and flats) in addition to the object frames. The images were also taken at multiple orientation angles of the telescope. They must either be unrotated before subtraction, or, as in the case of Fig. 1.5a–1.5b, they must be separated by orientation angle.

Dataset	Start Time	Exp Time	Instrument	Apertures	Filters/Gratings	Central Wavelength (Å)	Proposal ID
J8E730021	2003-03-26 2:28:55	2350	ACS	HRC-CORON1.8	CLEAR1S;F814W	8114.662	9295
J8E730031	2003-03-26 3:53:55	130	ACS	HRC-CORON1.8	F606W;CLEAR2S	5886.58	9295
J8E730041	2003-03-26 3:57:45	2600	ACS	HRC-CORON1.8	F606W;CLEAR2S	5886.58	9295
J8E730OVQ	2003-03-26 2:25:56	130	ACS	HRC-CORON1.8	CLEAR1S;F814W	8114.662	9295
J8E731011	2003-03-26 5:33:18	160	ACS	HRC-CORON1.8	CLEAR1S;F814W	8114.662	9295
J8E731021	2003-03-26 5:37:38	2520	ACS	HRC-CORON1.8	CLEAR1S;F814W	8114.662	9295
J8E731031	2003-03-26 7:05:50	130	ACS	HRC-CORON1.8	F606W;CLEAR2S	5886.58	9295
J8E731041	2003-03-26 7:09:40	2600	ACS	HRC-CORON1.8	F606W;CLEAR2S	5886.58	9295
J8QJ18011	2004-04-26 22:39:03	160	ACS	HRC-CORON1.8	CLEAR1S;F435W	4310.798	9987
J8QJ18021	2004-04-26 22:43:23	2400	ACS	HRC-CORON1.8	CLEAR1S;F435W	4310.798	9987
J8QJ18K0Q	2004-04-26 22:34:47	3	ACS	HRC	CLEAR1S;F435W	4310.798	9987
J8QJ18K1Q	2004-04-26 22:36:34	1	ACS	HRC-ACQ	CLEAR1S;F660N	6602*	9987
J8QJ19011	2004-04-26 23:54:24	160	ACS	HRC-CORON1.8	CLEAR1S;F435W	4310.798	9987
J8QJ19021	2004-04-26 23:58:44	2530	ACS	HRC-CORON1.8	CLEAR1S;F435W	4310.798	9987
J8QJ19K7Q	2004-04-26 23:51:55	1	ACS	HRC-ACQ	CLEAR1S;F660N	6602*	9987

Table 2.1 Specifications of the observations of HD100546 corresponding to Hubble Space Telescope proposal 9295 and 9987. Note that the two starred values in the Central Wavelength Column (valued at 6602) were originally listed at values of 0. The ACS Instrument Handbook lists the central wavelength for the F660N filter to be 6602Å, which has been included in the table.

The model PSF was constructed using images from another set of frames, known as the basis set. Basis images are gathered from every proposal taken with the HRC-CORON1.8 aperture in the F606W;CLEAR2S filter set. From the set of 289 images, 77 images were removed because they contained bad data (*i.e.* overexposed images, frames with no objects, etc.). The 212 remaining images were taken with a wide variety of parameters (integration time, object type, orientation angle, etc.). This variety allows us to accurately model the diffraction that comes from the instrumentation itself and not features from the objects being imaged.

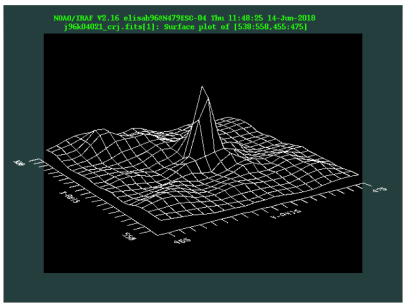

Figure 2.1 Standard PSF surface plot

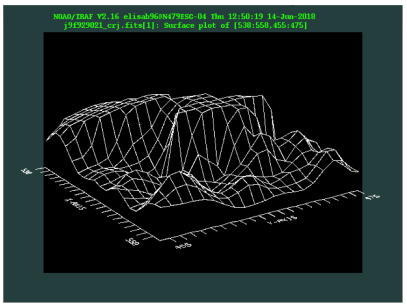

Figure 2.2 Cliff PSF surface plot

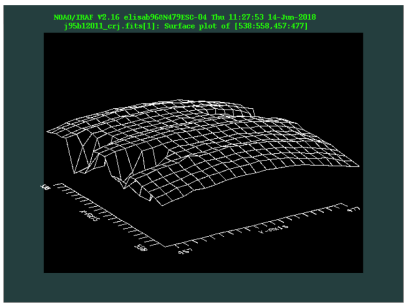

Figure 2.3 Dome PSF surface plot

The basis and object frames come from a variety of exposure times and must be sorted into various categories before being used to construct the PSF. The differences in exposure time create widely varied PSF shapes for the same object, as can be seen in Figures 2.1-3. Fig. 2.1 has been exposed the shortest, Fig. 2.2 for longer time, and Fig. 2.3 for the longest amount of time. Exposing for longer times oversaturates the center of the image, losing detail in the central regions of the PSF (Fig. 2.3). However, the longer exposures allow the fainter outer regions of the PSF to be observed in more detail. The combination of different PSF types could obscure planets within the disk, so a separate model PSF must be created using each individual PSF type. Sorting by type is accomplished by generating a surface plot of each image in IRAF (a data reduction software) and determining its category by eye. The surface plots tend to be one of three shapes: a standard PSF (Figure 2.1), a "cliff" (Figure 2.2), or a "dome" (Figure 2.3). Appendix A contains a table (Table A.1) that details which images were placed in each category. These categories are important to our PSF modeling techniques, which are further discussed in Section 2.2.

2.2 PSF Subtraction

The first step of PSF subtraction is to model the general diffraction due to the coronagraphic mask. Stacking a large number of images taken with the same instrument and filter set creates the model

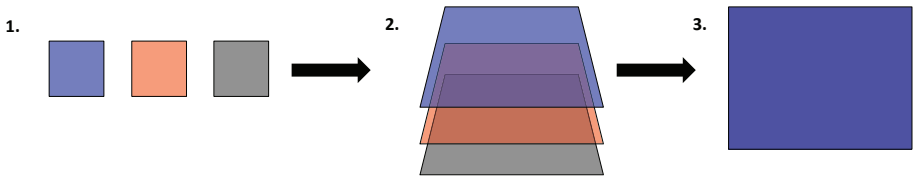

Figure 2.4 Representation of the stacking of basis images . (1) Coronagraphic images from a number of different objects are selected. (2) Images are aligned prior to stacking. (3) A composite image is generated from the stacked images.

PSF. Figure 2.4 shows a representation of the stacking process. First, a series of images are selected. For our object, the set includes all images taken by HST with the HRC-CORON1.8 aperture and F606W;CLEAR1S filter set (basis frames). These images are then sorted according to the PSF types discussed in Section 2.1. After the desired images and types are chosen, the images must be aligned properly to prevent loss of detail in the PSF. Finally, the images are stacked and combined to create a composite image that models the diffraction due to instrumentation.

In constructing our model PSF , we expect the stack of PSF shapes (*c.f.* Fig. 2.1–2.3) that most closely resemble the object frames to yield the best result. Therefore, if the science frame falls into the "standard PSF" category, we use the "standard basis" image set.

2.3 PynPoint

The program PynPoint[1] is a Python based software that both creates a model PSF from a set of basis images and subtracts the model from the object frames. Most software packages of this type are designed for ground-based work, or written to work exclusively with a specific set of instruments. PynPoint was chosen over other PSF subtraction softwares because it is adaptable for space-based observations, such as the HST data. Additionally, PynPoint is freely available to the public and widely used for PSF subtraction. It has been well tested and was used for many exoplanetary

[1] https://pynpoint.readthedocs.io/en/latest/

discovery papers (Quanz 2015). An end-to-end example of a complete run of PynPoint is included in Appendix **??**.

Principle Component Analysis (PCA) is the statistical process that PynPoint uses to perform PSF subtraction. PCA is a machine learning technique that maps topographical features of the PSF to the object frames using eigenvalues and eigenvectors. However, the PCA algorithm that PynPoint uses is highly aggressive and can generate false positives within the residual images.

PynPoint works with several different data types, including science frames and Fdh5 data cubes. Science frames come in the form of Flexible Image Transport System (FITS) files. FITS files contain a header which tells the specifications of the image—such as filter, exposure length, object name, etc.— and a number of file extensions. For the purpose of this project, we only used the first extension which contains the object frame. FITS files are 2-D arrays of pixels, whereas the Fdh5 data cubes are an "n-D" array of pixels. In PynPoint, the Fdh5 cubes contain all of the information used to perform the PSF subtraction. The user creates an Fdh5 cube by reading in all data that will be analyzed in any given run of the program. This includes the science frames, basis frames, model PSF, and any other frames necessary for reduction. The cube tracks the changes made to any of the images, as well as storing the final residual image output.

To use PynPoint, the user creates a custom pipeline containing any number of modules. Modules are functions that typically come preprogrammed in PynPoint, although the user does have the option of writing their own. To generate a pipeline, the user defines an instance of "pypeline", and then uses a number of functions to add and subtract customized modules to the pipeline. The pipeline will run the modules in the order that they are added. Once the pipeline is completed, it can then be run and residual images will be generated.

The first modules created in PynPoint are the FITS reading modules. These modules read the science and basis frames from a specified directory and adds them to the Hdf5 cube generated by PynPoint. Each FITS reading module is written with an accompanying "tag", which specifies what

the frames will be used for in the analysis. The tags are used in many modules to specify which group of images to run a module on. A separate module must be written for the basis and science frames in order to associate them with separate tags.

Object frames must be properly aligned before the model PSF can be subtracted from them to avoid generating false positives or inadvertently removing a planet from the residuals. The "StarCenteringModule" in PynPoint, which uses a 2-D Gaussian profile to align the central peak of the PSF feature (Figure 2.1), produced the best centering result. The most important parameter in this module is the radius within which the module searches. This parameter is measured in arcseconds, so the appropriate range of pixels to search must be determined by the plate scale of the images. For our ACS data, each pixel covers ~0.025 arcseconds of the sky. The size of the search area was set to 2 arcseconds, which means that an 80x80 pixel range was covered in the center of the image. Although this may seem like a large range of pixels, it only covers ~1.5% of the total image.

Magnification of images before alignment can cause better alignment to take place. Magnification is accomplished with the "ScaleImagesModule", which utilizes a spline interpolation algorithm. Essentially, each pixel is expanded into an *nxm* pixel array, where *n* and *m* are the magnification factors of the horizontal and vertical dimensions of the image, respectively. Once split, the interpolation will assign an intensity value to each pixel based on the value of the surrounding pixels. Magnifying the images before aligning them allows for a more finely detailed alignment to take place. After alignment, the images are then be scaled back down to their original size.

To create the model PSF, the basis images must also be aligned before stacking. This is done the same way that the science frames were aligned. To stack the images and create the model PSF, you simply use the "DerotateAndStackModule". However, the rotation function in this module must be turned off. This function uses the parallactic angles of the telescope, which are essential for ground-based observations. Parallactic angles track the rotation of the telescope as it tracks

an object across the sky. Space-based observations do not have parallactic angles, therefore this function is unnecessary for our purposes.

Before subtraction, all the images must go through a final round of preparations. As opposed to older versions of PynPoint which required all the steps to be done individually, the newest version of PynPoint allows all of these steps to be taken with a singular module: the "PSFPreparationModule". This module resizes, masks, and normalizes the images in preparation for the PCA subtraction. The mask is used to indicate the dimensions of the coronagraph, which, as seen in Fig. 1.3, can remove a central portion of the images. The images can be resized to any scale, but typically they are magnified by a factor of two. The images are normalized so that the difference in intensity of the basis stack and the intensity of the science frames does not impact the subtraction.

The residual images produced from the subtraction show deviation from the mean disk brightness. Objects much brighter than the disk should show up as speckles within the residual image. However, the nature of the data means that the residual images contain a lot of noise. The noise, combined with the fact that the PCA process PynPoint employs is highly aggressive, makes the detection of any exoplanets within the disk dubious. However, as the main purpose of this analysis is to screen for potential exoplanet detections, we can use these residuals as justification to apply for telescope time.

Chapter 3

Results

3.1 Analysis and Conclusions

The purpose of my research was to recreate and confirm the detection of HD100546b and HD100546c by previous student Emily Safsten, as discussed in section 1.3 (Safsten Brigham Young University, Provo, U.T., 2017). The detection of HD100546b would be exciting because it would prove the validity of using archival data as a screening technique for finding planetary companions, but the additional detection of HD100546c would be groundbreaking as it is currently unconfirmed. It is highly unlikely that HD100546c would be detected without HD100546b, so the focus of the analysis was primarily on confirming Safsten's detection of the known planet (HD100546b). Unfortunately however, the detection made by Safsten is most likely a false positive generated by the aggressive PCA analysis employed by PynPoint.

The archival ACS data used in our subtraction is not optimized for observing planets. Because the data was originally intended to provide insight into the structure of the disk itself and not to image planets, the residual images produced are incredibly noisy. It can be difficult to distinguish the signature of a planet from the noise produced by the disk itself. Additionally, the filters used to

take the data are problematic. The data were taken in optical wavelengths centered at 606μm and 814μm. While optical data is perfect for investigating disk features, planets typically emit most of their light in infrared. It is possible that a detection can be made in optical wavelengths, though it is much more difficult to achieve. If HD100546b is detected in optical wavelengths, it is most likely due to reflected light from the host star and not the blackbody emission of the planet. Detections with reflected light are highly unusual, so as exciting as this detection would be it is simply one more reason to doubt the subtraction performed by Safsten (2017).

The angular separation of HD100546c and the host star may not be large enough to resolve in the ACS data. At a proposed distance of only 14AU, HD100546c is comparatively close to the central regions of the disk. At this distance it is likely that the PSF from the star will overtake the signal from HD100546c. Much of the detail at this region of the disk is likely lost due to the limits of the instrumentation. If this is the case, HD100546c should not be detectable in the residual images. On the other hand, at a distance of 50AU from the central star, HD100546b is easily resolvable with HST and should appear in the residuals. This is a point in favor of the subtraction Safsten completed.

The difference between the two images produced by Safsten's subtractions, as seen in Figure 1.5a and Figure 1.5b, is the orientation angle of the telescope. Changing the orientation angle of the telescope can help probe different regions of the protoplanetary disk. The structure of the optics in the telescope and coronagraphic mask can obscure sections of the protoplanetary disk. Rotating the telescope changes the sections that are blocked, and thus reveals new information about the disk. Nevertheless, it is suspicious that HD1000546b appears in one image, and HD100546c in another. It is highly unlikely that the optics would perfectly obscure a different planet at each orientation angle. This is additional evidence that Safsten's subtraction did not produce a real detection of HD100546b.

Categorizing the science and basis frames by the three different PSF types is essential to

producing an accurate subtraction (*c.f.* Sec. 2.2). However, this preliminary step was not taken by Safsten in producing her subtraction. The model PSF is therefore inaccurate, and the subtraction is likely incorrect.

After considering the many reasons to doubt Safsten's subtraction, we have concluded that it is most likely a false positive. However, because HD100546b has been confirmed (Quanz 2015) we believe that it can be detected within the ACS data.

3.2 Directions for Further Work

With further work, a detection of HD100546b may be obtained. We are currently refining the methods Safsten used to generate a better PSF subtraction. This includes a deep investigation of the images used to construct the model PSF, experimentation of different fitting algorithms (Gaussian profiles, spline interpolations, Fourier analysis, etc.), improved subtraction modules, and comparisons of HD100546 with other similar objects. An updated version of PynPoint was released in 2019 with improved PSF subtraction techniques (Stolker et al. 2019). The improved algorithms should allow us to detect the elusive HD100546b and, hopefully, HD100546c.

In addition to refining our subtraction methods, analyzing HD100546 in other filters is essential to confirming its detection. HD100546 has been observed in other filter sets with ACS that could be used to confirm these results. Most of this work was done using the F606W filter, but ACS has data in F814W and F435W. If the planet appears in all three filter sets it is very likely that it is a real detection. If our current efforts to improve the PSF subtraction are fruitful, the analysis of these additional filters could provide a concrete confirmation of HD100546b, and provide proof of concept for the archival data screening technique.

The Near Infrared Camera and Multi-Object Spectrometer (NICMOS) instrument on the Hubble telescope has also been used to observe HD100546. These observations were taken further into the

infrared which could increase the likelihood of a detection. If HD100546b and HD100546c can be detected within both the NICMOS and ACS data then the detections are very likely to be real.

With modern instruments it may now be possible to directly image HD100546c. To test this, we observed HD100546 using the Very Large Telescope (VLT). The filter used was the J8.9 filter, which is centered at 8.9μm. This filter was chosen to match the blackbody curve of HD100546b, which can be seen in Figure 3.1. The filters used to detect HD100546b by Quanz et al. (2015) are also seen in the figure. The blackbody curve peaks around 2.8μm and then slopes gently with increasing wavelength. The L' and M' filters are centered close to the peak of the blackbody, so they observe a large portion of the planet's light. However, the host star is also very bright at these wavelengths which makes the contrast between the objects difficult to discern. The J8.9 filter, on the other hand, is centered at a much longer wavelength. Although the planet is also giving out less light at these wavelengths, the star's blackbody curve falls off much faster, causing the ratio of the intensities to change. Observations with J8.9 would mean that the light of the host star is much less of a problem than they are in the L' and M' data sets. For cooler companions, such as the proposed HD100546c, this effect will be even more pronounced as their blackbody curves peak at longer wavelengths. Unfortunately, we did not get enough data from VLT within our observation window to obtain the signal to noise ratio (SNR) needed to image either planet. Submitting a second proposal to VLT or another Infrared based telescope could give us the data needed to detect HD100546c.

If the detection of HD100546b is confirmed, then using archival data to screen for planets with direct imaging could allow many more exoplanets to be discovered. HD100546 was chosen as a test subject for the screening method because it already contains a confirmed planet. If we can detect this planet within the optical archival data then we should be able to detect exoplanets in other systems using similar data. We could then screen the hundreds of objects stored in the HST archives for potential planetary companions that could then be confirmed with new observations. HST archives host a massive amount of data that, when revisited with modern processing techniques, could reveal

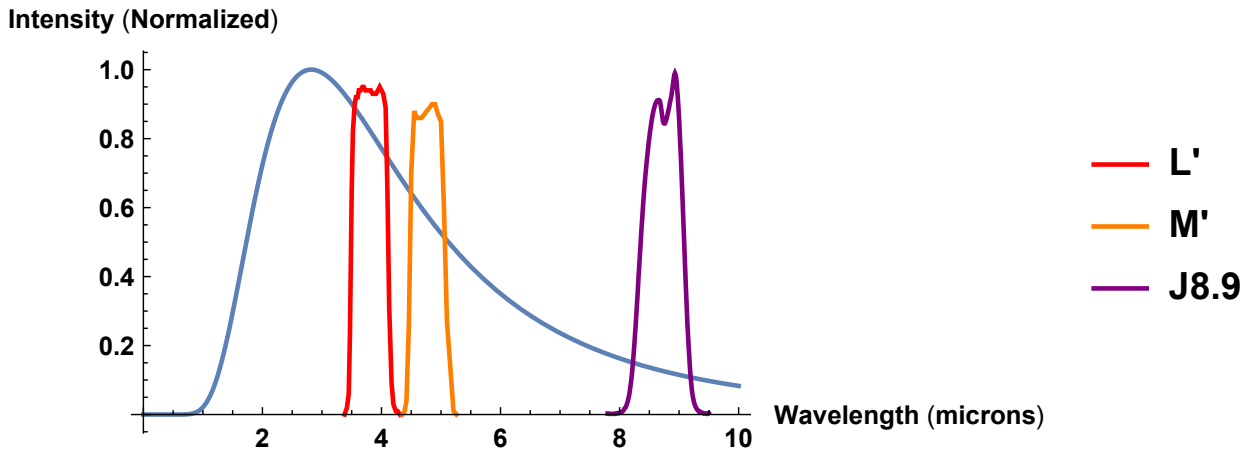

Figure 3.1 The normalized blackbody curve of HD100546b is shown in blue. The filter sets L' and M' used by Quanz, et al (2015) to detect HD100546b can be seen in red and orange respectively. The VLT filter J8.9 used in our proposal for telescope time is shown in purple.

a plethora of undiscovered exoplanets.

Appendix A

Basis Images

Table A.1 The results of the surface plot sorting of the basis images . This table records the observed object's name, the name of any images taken of that object, the exposure length in seconds, and PSF type.

Object Name	Image	Exposure Time (seconds)	PSF Type	Proposal ID
PI1-GRU	j6fn03021_ crj.fits	5.00E+02	Standard	9100
3C273	j8cw08011_ crj.fits	2.20E+03	Standard	8992
3C273	j8cw08041_ crj.fits	2.55E+03	Standard	8992
HD-105281	j8cw10021_ crj.fits	5.00E+02	Standard	8992
HD141569	j8cw11021_ crj.fits	2.06E+03	Standard	8992
HD141569	j8cw12021_ crj.fits	2.06E+03	Standard	8992
HD129433	j8cw13021_ crj.fits	4.20E+02	Standard	8992
HD-163296	j8e720031_ crj.fits	1.00E+02	Standard	9295
HD-163296	j8e721031_ crj.fits	1.00E+02	Standard	9295
HD-145570	j8e722041_ crj.fits	9.00E+02	Cliff	9295
HD-100546	j8e730031_ crj.fits	1.30E+02	Standard	9295
HD-100546	j8e731031_ crj.fits	1.30E+02	Standard	9295
HD-129433	j8e732041_ crj.fits	1.02E+03	Cliff	9295

HD38678	j8gi01011_ crj.fits	1.08E+03	Standard	9475
HD38678	j8gi01021_ crj.fits	7.65E+02	Dome	9475
HD38678	j8gi02011_ crj.fits	1.08E+03	Standard	9475
HD38678	j8gi02021_ crj.fits	7.65E+02	Dome	9475
HD95418	j8gi05011_ crj.fits	8.40E+02	Dome	9475
HD95418	j8gi05021_ crj.fits	1.08E+03	Dome	9475
HD102647	j8gi06011_ crj.fits	6.90E+02	Dome	9475
HD102647	j8gi06021_ crj.fits	9.80E+02	Dome	9475
HD139006	j8gi07011_ crj.fits	8.25E+02	Dome	9475
HD139006	j8gi07021_ crj.fits	9.00E+02	Dome	9475
HD157792	j8gi08011_ crj.fits	2.28E+03	Dome	9475
HD161868	j8gi09011_ crj.fits	2.24E+03	Dome	9475
HD17206	j8gi10011_ crj.fits	2.34E+03	Dome	9475
HD27290	j8gi11011_ crj.fits	2.46E+03	Dome	9475
HD128167	j8gi12011_ crj.fits	2.18E+03	Dome	9475
HD139664	j8gi13011_ crj.fits	2.18E+03	Dome	9475
HD142860	j8gi14011_ crj.fits	2.24E+03	Dome	9475
HD20794	j8gi15011_ crj.fits	2.14E+03	Dome	9475
HD30495	j8gi16011_ crj.fits	2.30E+03	Cliff	9475
HD48682	j8gi17011_ crj.fits	2.33E+03	Cliff	9475
HD84117	j8gi18011_ crj.fits	2.31E+03	Dome	9475
HD160691	j8gi19011_ crj.fits	2.25E+03	Cliff	9475
HD10476	j8gi20011_ crj.fits	2.34E+03	Cliff	9475
HD53143	j8gi22011_ crj.fits	2.34E+03	Standard	9475
HD201091	j8gi23011_ crj.fits	2.34E+03	Dome	9475
HD221354	j8gi24011_ crj.fits	2.34E+03	Standard	9475
HD80613	j8j806011_ crj.fits	1.65E+03	Standard	9667

HD79248	j8j8a6011_ crj.fits	1.65E+03	Standard	9667
HD-100453	j8qj01021_ crj.fits	2.48E+03	Standard	9987
HD-87427	j8qj02011_ crj.fits	2.00E+03	Cliff	9987
HD-107146	j8qj03021_ crj.fits	2.33E+03	Standard	9987
HD-191089	j8qj06011_ crj.fits	2.01E+03	Standard	9987
BETA-PIC	j8qj15031_ crj.fits	2.03E+03	Dome	9987
BETA-PIC	j8qj16031_ crj.fits	2.03E+03	Dome	9987
ALF-PIC	j8qj17061_ crj.fits	4.00E+02	Dome	9987
GJ-803	j8qj21021_ crj.fits	2.25E+03	Standard	9987
GJ-803	j8qj21061_ crj.fits	2.80E+03	Standard	9987
HD-216149	j8qj22021_ crj.fits	1.80E+02	Standard	9987
GJ-803	j91701011_ crj.fits	1.83E+03	Standard	10330
HD-216149	j91702021_ crj.fits	2.90E+02	Standard	10330
SIRTF-2	j91705031_ crj.fits	2.25E+03	Standard	10330
SIRTF-4	j91709031_ crj.fits	2.40E+03	Standard	10330
SIRTF-4-PSF	j91710031_ crj.fits	2.51E+03	Cliff	10330
SIRTF-5	j91711031_ crj.fits	2.50E+03	Standard	10330
HD-216435	j91719031_ crj.fits	2.30E+03	Cliff	10330
HD-92945	j91722011_ crj.fits	2.30E+03	Standard	10330
HD-92945	j91722041_ crj.fits	2.50E+03	Standard	10330
HD-92945	j91724011_ crj.fits	2.27E+03	Standard	10330
HD-92945	j91724021_ crj.fits	2.60E+03	Standard	10330
HD-105	j91726031_ crj.fits	2.30E+03	Standard	10330
HD109085	j93n10031_ crj.fits	1.00E+01	Standard	10244
HD109085	j93n10041_ crj.fits	2.28E+03	Dome	10244
HD109085	j93n11031_ crj.fits	1.00E+01	Standard	10244
HD109085	j93n11041_ crj.fits	2.28E+03	Dome	10244

HD105452	j93n12031_ crj.fits	1.00E+01	Standard	10244
HD105452	j93n12041_ crj.fits	2.30E+03	Dome	10244
HD172167	j95b10011_ crj.fits	3.00E+02	Dome	10390
HD172167	j95b10031_ crj.fits	1.44E+02	Dome	10390
HD216956	j95b11011_ crj.fits	3.20E+02	Dome	10390
HD216956	j95b11031_ crj.fits	3.00E+02	Dome	10390
HD216956	j95b11051_ crj.fits	3.40E+02	Dome	10390
HD216956	j95b12011_ crj.fits	3.20E+02	Dome	10390
HD216956	j95b12031_ crj.fits	3.00E+02	Dome	10390
HD216956	j95b12051_ crj.fits	3.40E+02	Dome	10390
HD216956	j95b13011_ crj.fits	3.20E+02	Dome	10390
HD216956	j95b13031_ crj.fits	3.00E+02	Dome	10390
HD216956	j95b13051_ crj.fits	3.40E+02	Dome	10390
HD210418	j95b15011_ crj.fits	7.80E+02	Dome	10390
HD210418	j95b15021_ crj.fits	1.34E+03	Dome	10390
HD172167	j95b20011_ crj.fits	3.00E+02	Dome	10390
HD172167	j95b20031_ crj.fits	1.44E+02	Dome	10390
HD216956	j95b21011_ crj.fits	3.20E+02	Dome	10390
HD216956	j95b21031_ crj.fits	3.00E+02	Dome	10390
HD216956	j95b22011_ crj.fits	3.20E+02	Dome	10390
HD216956	j95b22031_ crj.fits	3.00E+02	Dome	10390
HD216956	j95b23011_ crj.fits	3.20E+02	Dome	10390
HD216956	j95b23031_ crj.fits	3.00E+02	Dome	10390
HD210418	j95b25011_ crj.fits	7.80E+02	Dome	10390
HD210418	j95b25021_ crj.fits	1.34E+03	Dome	10390
HD20797	j96a06011_ crj.fits	1.05E+03	Cliff	10409
HD34282	j96k01021_ crj.fits	2.00E+02	Standard	10425

HD34282	j96k01031_ crj.fits	1.78E+03	Standard	10425
HD36863	j96k02011_ crj.fits	2.00E+02	Standard	10425
HD36863	j96k02021_ crj.fits	1.48E+03	Standard	10425
HD97048	j96k03021_ crj.fits	2.00E+02	Standard	10425
HD97048	j96k03031_ crj.fits	2.20E+03	Standard	10425
HD80999	j96k04011_ crj.fits	2.00E+02	Standard	10425
HD80999	j96k04021_ crj.fits	1.70E+03	Standard	10425
HD139450	j96k05021_ crj.fits	2.00E+02	Standard	10425
HD139450	j96k05031_ crj.fits	1.83E+03	Standard	10425
HD144766	j96k06011_ crj.fits	2.00E+02	Standard	10425
HD144766	j96k06021_ crj.fits	1.48E+03	Standard	10425
HD158643	j96k07011_ crj.fits	9.60E+01	Standard	10425
HD158643	j96k07021_ crj.fits	1.92E+03	Cliff	10425
HD159217	j96k08011_ crj.fits	1.80E+01	Standard	10425
HD159217	j96k08021_ crj.fits	2.09E+03	Cliff	10425
HD159492	j96k09011_ crj.fits	1.50E+02	Standard	10425
HD135379	j96k10011_ crj.fits	1.20E+01	Standard	10425
HD135379	j96k10021_ crj.fits	2.21E+03	Dome	10425
HD195627	j96k11011_ crj.fits	9.60E+01	Standard	10425
HD219571	j96k12011_ crj.fits	1.20E+01	Standard	10425
HD219571	j96k12021_ crj.fits	2.21E+03	Dome	10425
PSRJ0737-3039	j97301011_ crj.fits	2.50E+03	Standard	10411
PSRJ0737-3039	j97302011_ crj.fits	2.50E+03	Standard	10411
PSRJ0737-3039	j97303011_ crj.fits	2.50E+03	Standard	10411
GJ3305	j9bc01021_ crj.fits	2.29E+03	Standard	10487
GJ3305	j9bc01081_ crj.fits	2.00E+02	Standard	10487
GJ3305	j9bc01091_ crj.fits	2.07E+03	Standard	10487

HD28159	j9bc02011_ crj.fits	1.00E+02	Standard	10487
HD28159	j9bc02021_ crj.fits	2.04E+03	Standard	10487
CD-57D1054	j9bc03021_ crj.fits	2.52E+03	Standard	10487
CD-57D1054	j9bc03041_ crj.fits	2.00E+02	Standard	10487
CD-57D1054	j9bc03051_ crj.fits	2.35E+03	Standard	10487
BD+05D378	j9bc05021_ crj.fits	2.05E+03	Standard	10487
BD+05D378	j9bc05071_ crj.fits	2.00E+02	Standard	10487
BD+05D378	j9bc05081_ crj.fits	1.90E+03	Standard	10487
HD15685	j9bc06011_ crj.fits	2.10E+03	Standard	10487
BD+30D397A	j9bc07021_ crj.fits	2.21E+03	Standard	10487
BD+30D331	j9bc08011_ crj.fits	2.20E+03	Standard	10487
BD+30D397B	j9bc09021_ crj.fits	2.09E+03	Standard	10487
CD-64D1208	j9bc11021_ crj.fits	2.50E+03	Standard	10487
HD174429	j9bc17021_ crj.fits	2.46E+03	Standard	10487
HD178150	j9bc18011_ crj.fits	2.39E+03	Standard	10487
HD35850	j9bc19021_ crj.fits	1.00E+02	Standard	10487
HD35850	j9bc19031_ crj.fits	2.00E+03	Standard	10487
HD36379	j9bc20011_ crj.fits	1.00E+02	Standard	10487
HD36379	j9bc20021_ crj.fits	1.95E+03	Standard	10487
HD203	j9bc21021_ crj.fits	1.00E+02	Standard	10487
HD1343	j9bc22011_ crj.fits	1.00E+02	Standard	10487
HD1343	j9bc22021_ crj.fits	1.95E+03	Standard	10487
HD29391	j9bc23021_ crj.fits	1.00E+02	Standard	10487
HD32115	j9bc24011_ crj.fits	1.00E+02	Standard	10487
HD32115	j9bc24021_ crj.fits	1.90E+03	Standard	10487
HD155555C	j9bc25021_ crj.fits	2.61E+03	Standard	10487
HD155555C	j9bc25081_ crj.fits	2.44E+03	Standard	10487

HD171778	j9bc26011_ crj.fits	2.67E+03	Standard	10487
HD215120	j9bc28011_ crj.fits	2.45E+03	Standard	10487
HD209336	j9bc30011_ crj.fits	2.29E+03	Standard	10487
HD172555	j9bc35021_ crj.fits	1.00E+02	Standard	10487
HD172555	j9bc35031_ crj.fits	2.30E+03	Cliff	10487
HD165040	j9bc36011_ crj.fits	1.00E+02	Standard	10487
HD165040	j9bc36021_ crj.fits	2.31E+03	Dome	10487
HD146624	j9bc37021_ crj.fits	1.00E+02	Standard	10487
HD146624	j9bc37031_ crj.fits	2.04E+03	Dome	10487
HD142851	j9bc38011_ crj.fits	1.00E+02	Standard	10487
HD142851	j9bc38021_ crj.fits	1.98E+03	Standard	10487
HD31906	j9bc54011_ crj.fits	1.00E+02	Standard	10487
HD31906	j9bc54021_ crj.fits	2.31E+03	Standard	10487
BD+30D397B	j9bc59021_ crj.fits	2.09E+03	Standard	10487
BD+32D358	j9bc60011_ crj.fits	2.20E+03	Standard	10487
TAU-CETI	j9bw01011_ crj.fits	3.80E+01	Standard	10695
TAU-CETI	j9bw01021_ crj.fits	2.50E+02	Cliff	10695
TAU-CETI	j9bw01031_ crj.fits	1.67E+03	Dome	10695
HD-20794	j9bw02011_ crj.fits	1.00E+02	Standard	10695
HD-20794	j9bw02021_ crj.fits	2.08E+03	Dome	10695
HD-172051	j9bw03011_ crj.fits	2.00E+02	Standard	10695
HD-172051	j9bw03021_ crj.fits	2.05E+03	Cliff	10695
HD-173540	j9bw04021_ crj.fits	2.20E+03	Dome	10695
HD-205536	j9bw05021_ crj.fits	2.39E+03	Standard	10695
HD-219077	j9bw06011_ crj.fits	2.00E+02	Standard	10695
HD-202917	j9bw07011_ crj.fits	2.46E+03	Standard	10695
HD-202457	j9bw08011_ crj.fits	2.00E+02	Standard	10695

HD-126265	j9bw09021_ crj.fits	2.27E+03	Standard	10695
HIP-7805	j9f901021_ crj.fits	2.46E+03	Standard	10539
HIP-7805	j9f902011_ crj.fits	2.61E+03	Standard	10539
HD-113556	j9f904021_ crj.fits	2.44E+03	Standard	10539
HD-113556	j9f905011_ crj.fits	2.58E+03	Standard	10539
HD-101727	j9f906021_ crj.fits	2.57E+03	Standard	10539
HR-1082	j9f907021_ crj.fits	2.31E+03	Standard	10539
HD-15427	j9f909031_ crj.fits	2.14E+03	Cliff	10539
HD-167468	j9f912031_ crj.fits	2.40E+03	Cliff	10539
HD-82943	j9f917011_ crj.fits	2.42E+03	Standard	10539
HD-84117	j9f918031_ crj.fits	2.03E+03	Cliff	10539
HD-38206	j9f919031_ crj.fits	2.08E+03	Standard	10539
HD-38206	j9f920021_ crj.fits	2.20E+03	Standard	10539
HD-41695	j9f921021_ crj.fits	1.00E+02	Standard	10539
HD-41695	j9f921031_ crj.fits	1.95E+03	Cliff	10539
HD-7570	j9f927021_ crj.fits	1.00E+02	Standard	10539
HD-7570	j9f927031_ crj.fits	1.97E+03	Cliff	10539
HD-207129	j9f929021_ crj.fits	2.08E+03	Cliff	10539
HD-211415	j9f930021_ crj.fits	1.00E+02	Standard	10539
HD216956	j9fq09031_ crj.fits	6.00E-01	Standard	10598
HD216956	j9fq10031_ crj.fits	6.00E-01	Standard	10598
HD216956	j9fq11031_ crj.fits	6.00E-01	Standard	10598
HD172167-PSF	j9fq12041_ crj.fits	3.12E-01	Standard	10598
HD216956	j9fq13031_ crj.fits	6.00E-01	Standard	10598
HD172167-PSF	j9fq14041_ crj.fits	3.12E-01	Standard	10598
HD-139664	j9gh11031_ crj.fits	1.57E+03	Dome	10599
HD-139664	j9gh12031_ crj.fits	1.57E+03	Dome	10599

HD-142860-PSF	j9gh13021_ crj.fits	9.00E+02	Dome	10599
HD-142860-PSF	j9gh14021_ crj.fits	9.00E+02	Dome	10599
HD-15745	j9ps06021_ crj.fits	2.10E+03	Standard	10896
HD-68456	j9ps11021_ crj.fits	2.10E+03	Dome	10896
HD-122652	j9ps15021_ crj.fits	2.10E+03	Standard	10896
HD-117176	j9ps25021_ crj.fits	2.10E+03	Dome	10896
HIP-13005	j9ps27021_ crj.fits	2.10E+03	Standard	10896
HD-128311	j9ps29021_ crj.fits	2.10E+03	Standard	10896
PSF-HD-129312	j9ps30021_ crj.fits	2.10E+03	Dome	10896

Bibliography

Currie, T., et al. 2014, The Astrophysical Journal Letters, 796

Espaillat, C. 2019, in American Astronomical Society Meeting Abstracts, Vol. 233, American Astronomical Society Meeting Abstracts #233, 421.01

Guimarães, M. M., Alencar, S. H. P., Corradi, W. J. B., & Vieira, S. L. A. 2006, A&A, 457, 581

Quanz, S. P. 2015, Astrophys Space Sci

Quanz, S. P., Amara, A., Meyer, M. R., Girard, J. H., Kenworthy, M. A., & Kasper, M. 2015, The Astrophysical Journal, 807

Quanz, S. P., Amara, A., Meyer, M. R., & Kenworthy, M. A. 2013, The Astrophysical Journal Letters, 766

Safsten, E. Brigham Young University, Provo, U.T., 2017, Masters Thesis

Stolker, T., Bonse, M. J., Quanz, S. P., Amara, A., Cugno, G., Bohn, A. J., & Boehle, A. 2019, A&A, 621, A59

van den Ancker, M. E., The, P. S., Tjin A Djie, H. R. E., Catala, C., de Winter, D., Blondel, P. F. C., & Waters, L. B. F. M. 1997, A&A, 324, L33

Index

archival data, 7, 8, 10, 11, 18, 20, 21

basis images, 5, 12–15, 23

coronagraph, 4, 5, 7, 10, 11, 13, 14, 17

HD100546b, 6, 7, 9, 18–21
Herbig Ae/Be stars, 2, 4, 6, 8, 11
Hot Jupiter, 2

Image Magnification, 16

Pipeline, 15
Point Spread Function (PSF), 4, 5, 10, 14
Principle Component Analysis (PCA), 15, 18
protoplanetary disk, 1–6, 8, 10, 11, 18, 19
PSF subtraction, 5, 7, 10, 11, 13–17, 20
PynPoint, 11, 14, 15, 17, 18, 20